Dual SIFamide receptors in Ixodes salivary glands

Fetta Guerrib, Caina Ning, Lourdes Mateos-Hernandéz, Sabine Rakotobe, Yoonseong Park, Ondrej Hajdusek, Jan Perner, Marie Vancová, James Valdés, Ladislav Šimo

Insect Biochemistry and Molecular Biology 158 (2023) 103963

Contents lists available at ScienceDirect

Insect Biochemistry and Molecular Biology

journal homepage: www.elsevier.com/locate/ibmb

Dual SIFamide receptors in *Ixodes* salivary glands

Fetta Guerrib [a], Caina Ning [a], Lourdes Mateos-Hernandéz [a], Sabine Rakotobe [a], Yoonseong Park [b], Ondrej Hajdusek [c], Jan Perner [c], Marie Vancová [c,d], James J. Valdés [c], Ladislav Šimo [a,*]

[a] ANSES, INRAE, Ecole Nationale Vétérinaire d'Alfort, UMR BIPAR, Laboratoire de Santé Animale, 94700, Maisons-Alfort, France
[b] Entomolgy department, Kansas State University, 123 Waters Hall, 66506-4004, Manhattan, KS, USA
[c] Institute of Parasitology, Biology Centre, Czech Academy of Sciences, Branišovská 31, 37005, České Budějovice, Czech Republic
[d] Faculty of Science, University of South Bohemia, České Budějovice, 37005, Czech Republic

ARTICLE INFO

Keywords:
SIFamide
SIFamide receptors
Ticks
Salivary gland acini
Synganglion

ABSTRACT

Salivary glands are vital to tick feeding success and also play a crucial role in tick-borne pathogen transmission. In previous studies of *Ixodes scapularis* salivary glands, we demonstrated that saliva-producing type II and III acini are innervated by neuropeptidergic axons which release different classes of neuropeptides via their terminals (Šimo et al., 2009b, 2013). Among these, the neuropeptide SIFamide—along with its cognate receptor—were postulated to control the basally located acinar valve via basal epithelial and myoepithelial cells (Vancová et al., 2019). Here, we functionally characterized a second SIFamide receptor (SIFa_R2) from the *I. scapularis* genome and proved that it senses a low nanomolar level of its corresponding ligand. Insect SIFamide paralogs, SMYamides, also activated the receptor but less effectively compared to SIFamide. Bioinformatic and molecular dynamic analyses suggested that *I. scapularis* SIFamide receptors are class A GPCRs where the peptide amidated carboxy-terminus is oriented within the receptor binding cavity. The receptor was found to be expressed in *Ixodes ricinus* salivary glands, synganglia, midguts, trachea, and ovaries, but not in Malpighian tubules. Investigation of the temporal expression patterns suggests that the receptor transcript is highly expressed in unfed *I. ricinus* female salivary glands and then decreases during feeding. In synganglia, a significant transcript increase was detected in replete ticks. In salivary gland acini, an antibody targeting the SIFa_R2 recognized basal epithelial cells, myoepithelial cells, and basal granular cells in close proximity to the SIFamide-releasing axon terminals. Immunoreactivity was also detected in specific neurons distributed throughout various *I. ricinus* synganglion locations. The current findings, alongside previous reports from our group, indicate that the neuropeptide SIFamide acts via two different receptors that regulate distinct or common cell types in the basal region of type II and III acini in *I. ricinus* salivary glands. Our study investigates the peptidergic regulation of the *I. ricinus* salivary gland in detail, emphasizing the complexity of this system.

1. Introduction

G protein-coupled receptors (GPCRs) constitute the largest family of transmembrane proteins in the animal kingdom that transduce extracellular signals to activate distinct intracellular responses (Pierce et al., 2002). In arthropods, GPCRs, along with their ligands, mediate a variety of major physiological processes, e.g., growth, reproduction, development, feeding, molting, homeostasis, metabolism, and behavior (Caers et al., 2012; Pietrantonio et al., 2018). Of the six GPCR classes, class A GPCRs (rhodopsin-like) bind peptides at opposing terminal conformations. Current knowledge on peptide terminal orientation concerns 25 residue positions within the GPCR binding cavity (Tikhonova et al., 2019). For instance, the hydrophilic Q134$^{3.32}$ residue of the human orexin-2 receptor (Ox2R) at the GPCR binding cavity is essential for interacting with the amidated peptide C-terminus (Hong et al., 2021). The Q$^{3.32}$ residue position is highly conserved among class A GPCRs that bind peptides in a similar manner. Conversely, if this class A GPCR residue position is acidic (D$^{3.32}$ or E$^{3.32}$), peptides will bind with the opposing N-terminus (Tikhonova et al., 2019).

Multiple orthologs of invertebrate and vertebrate GPCRs have been molecularly characterized and functionally tested following the release of genomic sequence data from the black-legged tick *I. scapularis* (Gulia-Nuss et al., 2016). Current research has primarily focused on identifying neuropeptides and neurotransmitter GPCRs that regulate tick salivary gland activity (Kim et al., 2018; Mateos-Hernandéz et al.,

* Corresponding author.
E-mail address: ladislav.simo@vet-alfort.fr (L. Šimo).

https://doi.org/10.1016/j.ibmb.2023.103963
Received 8 December 2022; Received in revised form 5 May 2023; Accepted 13 May 2023
Available online 29 May 2023

Abbreviations

E	esophagus
EC	basal epithelial cell
GC	granular cell
IR	immunoreactivity
MD	molecular dynamics
MIP	myoinhibitory peptide
OL	olfactory lobe
Ox2R	orexin-2 receptor
OsDM	opistosomal dorsomedial neuron
OsVM	opistosomal ventromedial neuron
PcSG	protocerebral neurons innervating salivary glands
PcDL	protocerebral dorsolateral neuron
PcDM	protocerebral dorsomedial neuron
PdDM	pedal dorsomedial neuron
SIFa_R	SIFamide receptor
SIFa_R1	SIFamide receptor 1
SIFa_R2	SIFamide receptor 2

2020a; Šimo et al., 2011, 2013, 2014b). Tick salivary glands play a pivotal role during feeding, as a plethora of active saliva components suppress and modulate the vertebrate host immune responses while facilitating bloodmeal acquisition (Mans, 2019; Perner et al., 2020; Šimo et al., 2017). Saliva-mediated suppression of local host immune responses proximal to the tick bite site enables tick-borne pathogens to either enter the host bloodstream or be acquired by the tick (Šimo et al., 2017). Furthermore, salivary glands act as key osmoregulatory organs that mediate water homeostasis by eliminating excessive fluid and waste, thus concentrating the essential nutrients of the bloodmeal for use in further tick development or fecundity (Kaufman and Phillips, 1973; Kim et al., 2019).

In *I. scapularis* salivary glands, neuropeptides—myoinhibitory peptide (MIP), SIFamide, and elevenin—are delivered via the axons of two giant protocerebral neurons (PcSG) to the basal regions of saliva-producing type II and III granular acini (Kim et al., 2018; Šimo et al., 2009b). A cognate receptor for each of these neuropeptides is expressed in this tissue (Kim et al., 2018; Šimo et al., 2013), with Vancová providing the most detailed description of SIFamide and its receptor (Vancová et al., 2019). Specifically, immunogold labeling revealed an association of SIFamide-releasing axons with basal epithelial cells (ECs) and single myoepithelial cells (MC), both overlying the arm of acinar valves in type II and III acini. The same report confirmed the expression of postsynaptic SIFamide receptors (called SIFa_R1 in this study) on both of these cell types, thus it has been suggested that SIFamide and its receptor regulate the release of saliva from the acinus to associated ducts by controlling the acinar valve (Vancová et al., 2019).

The first SIFamide receptor (SIFa_R) was functionally characterized in *Drosophila* (Jørgensen et al., 2006) followed by its SIFamide neuropeptide ligand, both of which are strongly evolutionarily conserved across invertebrate taxa (Verleyen et al., 2004). The SIFamide precursor of many arthropod species, including ticks, contains a sole copy of a mature neuropeptide, varying by a single amino acid at the N-terminus among differing species (Šimo et al., 2013). Its bioactivity has been directly linked to various physiological mechanisms e.g. modulation of sexual behavior, feeding-related physiological processes, hindgut motility, or sleeping (Dreyer et al., 2019; Martelli et al., 2017; Sellami and Veenstra, 2015; Šimo and Park, 2014; Terhzaz et al., 2007). Over the last decade, a dramatic expansion of transcriptomic and genomic sequence data from multiple arthropod species has intensified efforts to undertake comprehensive bioinformatic analysis of GPCRs. As a result of these endeavors, a recent study discovered that the genomes of several arthropods—including *I. scapularis*—contained a gene encoding a putative second SIFamide-like receptor (Veenstra, 2021). The same study hypothesized that the neuropeptide SIFamide and/or its recently discovered paralogs—SMYamides, that were identified in some insect species—could serve as the ligands of this receptor.

Here, we functionally characterized a second *I. scapularis* SIFamide receptor (SIFa_R2), and along with the previously-identified *I. scapularis* SIFa_R1 (Šimo et al., 2013), tested their affinity to the endogenous SIFamide ligand, as well as its insect paralogs. We also investigated the temporal expression pattern of SIFa_R2 in *I. ricinus* salivary glands and synganglia over the course of *I. ricinus* female feeding. Lastly, the generation of an anti-*I. ricinus/I. scapularis* SIFa_R2 antibody enabled us to localize the receptor to a specific cell type within *I. ricinus* salivary glands and synganglia. The present study functionally identifies a second SIFa_R and suggests its biological function in *I. ricinus* salivary glands.

2. Materials and methods

2.1. Ticks and experimental animals

I. ricinus adults were obtained from the *Ixodes* rearing facility of UMR-BIPAR, Maisons-Alfort, France and Parasitology Institute, České Budějovice, Czech Republic. Ticks were maintained in plastic vials containing sterile wood shavings in an incubator (PHCbi, Japan) at >90% relative humidity at 22 °C with a 12 h/12 h light-dark cycle. Adult ticks were fed on New Zealand rabbits (Almazán et al., 2018), mice (Mateos-Hernández et al., 2020b), or guinea pigs. The protocols using animals for tick feeding were approved by the ComEth Anses/ENVA/UPEC Ethics Committee for Animal Experimentation, (permit No. APAFIS #35511–2022022111197802 v2). Within the Parasitology Institute in the Czech Republic, all laboratory animals were treated in accordance with the Animal Protection Law of the Czech Republic No. 246/1992 Sb. (regulation 419/2012) and ethics approval No. 13/2021-P and were held in a facility accredited by the Ministry of Agriculture No. 4253/2019-MZE-17214 and 1643/2019-MZE-17214.

2.2. Sequence analysis and phylogeny

The protein sequences of a putative arthropod SIFa_R2, including *I. scapularis* sequence (XP_029828900), were described in a recent publication by Veenstra (2021). BLAST searches of arthropod genomes or transcriptomes were performed using NCBI databases (www.ncbi.nlm.nih.gov). For phylogenetic analysis, the ClustalW program from MEGA11 software was used to align the transmembrane region of GPCRs, followed by the neighbor-joining tree method, with 500 bootstrap replications (Tamura et al., 2021). Exon–intron coordinates of *I. scapularis* SIFa_R2 open reading frame (ORF) were obtained by aligning the GenBank ORF sequence XM_029973040 against the *I. scapularis* genome in Vectorbase (www.vectorbase.org). Graphical exon–intron distances were generated using the Exon–Intron Graphic Marker version 4 (WormWeb.org) and the image was refined in Adobe Photoshop version 24.0.1 (Adobe Inc.). Graphical visualization of transmembrane receptor was performed using Protter 1.0 (https://wlab.ethz.ch/protter/start/). Alignment of putative tick SIFamide receptors was performed using the MegAlignPro 17.3 tool in DNASTAR (www.dnastar.com). Identity and similarity between sequences was obtained by ClustalW analysis (http://npsa-pbil.ibcp.fr). Putative *I. ricinus* SIFa_R1 and SIFa_R2 sequences were obtained from Bioproject PRJNA657487 via the NCBI database.

2.3. Functional receptor assays

A putative ORF sequence of *I. scapularis* SIFa_R2 (XP_029828900) was chemically synthesized and inserted into a pcDNA3.1+ expression vector following the addition of a Kozak site (GCCGCCACC) before the translation initiation codon (Biomatik Cambridge, Canada). To express

I. scapularis SIFa_R1 (AGE11606) we used the construct SIFa_R1/pcDNA3.1+ as generated in Šimo et al. (2013). To monitor ligand-triggered calcium mobilization upon receptor activation as described in (Mateos-Hernandéz et al., 2020a; Šimo et al., 2013) we transiently expressed the receptor with human cytoplasmic aequorin (Vernon and Printen, 2002) in Chinese hamster ovary cells (CHO–K1, Sigma). Bioluminescent assays were performed in opaque 96-well plates (Nunc) using the Fluostar Omega microplate reader (BMG Labtech). Obtained luminescent values were analyzed using Excel (Microsoft Office), and the half maximum response values (EC_{50})—including dose-response curve generation—were calculated using the GraphPad Prism 5 software package (GraphPad Software, La Jolla California USA). The ligands used in the assay, *I. scapularis* SIFamide (AYRKPPFNGSIFamide) (Šimo et al., 2009b) and SMYamide of *Blattella germanica* (NPGVPFRRLPFNGSMYamide), *Locusta migratoria* (EGIAFQKLPFNGAMYamide), and *Medauroidea extradentata* (YNLRVPMNGGMYamide) (Veenstra, 2021), and an IMFamide of *Bombyx mori* (NYKNAPMNGIMFamide) (Roller et al., 2008) were synthesized with >80% purity (LifeTein, USA or Biomatik Cambridge, ON Canada). Negative controls consisted of mock transfections using only the aequorin reporter. Four and three biological replicates were performed for SIFa_R2 and SIFa_R1 assays, respectively, with three technical replicates for each ligand. To confirm the specificity of SIFamide/SIFa_R2 affinity, SIFa_R2 transfected cells were treated with three other *I. scapularis* neuropeptide ligands (5 μM concentration) such as: kinin (DTFGPWGamide) (Šimo et al., 2014a), natalisin (SPDGDTPPPGFVGARamide) (Mateos-Hernández et al., 2021), and elevenin (LDCRKYPFYYRCRGISA) (Kim et al., 2018).

2.4. In-silico protein-peptide binding and dynamics

Both *I. scapularis* SIFa_Rs protein models were constructed based on multiple, homologous resolved structures from the Protein Databank (PDB (Berman et al., 2000); queried by the I-TASSER server (Yang and Zhang, 2015). Each I-TASSER-predicted tertiary structure was submitted to the HPEPDOCK server, a hierarchical algorithm for *in-silico* protein-peptide binding designed for peptide flexibility (Zhou et al., 2018). The SIFamide peptide was submitted using the primary sequences in FASTA format. The top bound structures for each SIFa_R-peptide complex were chosen for further processing based on two criteria: (a) the peptide C-terminus was oriented towards the GPCR binding cavity and, (b) a favorable HPEPDOCK binding score. The SIFa_R-peptide complexes were then prepared and optimized using the Maestro software package (Schrödinger, 2021–1). Firstly, the SIFamide peptide C-terminal amide was added, and the disordered *I. scapularis* SIFa_R C-termini were truncated and capped with an *N*-methyl amide group. Secondly, the hydrogen atoms were replaced, and local minimizations were performed to remove any steric clashes. Thirdly, the hydrogen-bond networks were optimized with the Protein Preparation Wizard (Sastry et al., 2013). Lastly, the SIFa_R-peptide complexes were solvated in a 10 $Å^3$ orthorhombic box with a TIP3P water model (Jorgensen et al., 1983; Mahoney and Jorgensen, 2000), neutralized, salted with 0.15 M NaCl, and embedded in a phosphatidylcholine (POPC) bilayer. The CHARMM36 force field (Huang and MacKerell Jr, 2013) was used to parameterize the protein-peptide complexes, ions, and POPC membrane. Molecular dynamic (MD) simulations were all performed with a GPU-accelerated workstation running Desmond software (Bowers et al., 2006). According to the protein model refinement designed by (Zhu et al., 2008), each parameterized system was first refined by running 10 × 5 ns MD simulations using the Desmond default protocol. The Desmond protocol involves several initial equilibration steps and a final MD production stage conducted under isotropic conditions with an NPT ensemble coupled with a Nose-Hoover thermostat (Evans and Holian, 1985) and a Martyna-Tobias-Klein barostat (Martyna et al., 1994). The temperature was set at 300 K with a RESPA (Tuckerman et al., 1992) integrator at an inner time step of 2-fs. Images were captured using the Maestro software package (Schrödinger, 2022–1). Residue interactions were inspected using the H-bond contacts plugin from the Visual Molecular Dynamics program (Humphrey et al., 1996). The distance cutoff was set at 3.5 Å with a 90° angle threshold and detailed information for residue pairs.

2.5. Tissue-specific and quantitative real-time reverse transcriptase PCR (qRT-PCR)

Total RNA from various organs was extracted using Trizol reagent (Invitrogen) from four-day-fed *I. ricinus* females: salivary glands, synganglia, ovaries, trachea, midguts/hindguts, Malpighian tubules, and carcasses (ventral cuticle with legs, muscles, and fat bodies). The obtained RNA was reverse transcribed to cDNA using Superscript III (Invitrogen) and was used for classical PCR amplification. The primers used were 5′-TACTCGGTCGTGTTCGTCGT-3′ for forward and 5′-GATCCATGGTCCAAAGAGAT -3′ for reverse. The primer positions within the alignment of *I. ricinus sifa_r1* and *sifa_r2* ORFs (identity of 57.9%) as well as sequence and sequencing chromatograms (Eurofins) of the *sifa_r2* PCR amplicon are shown in Supplementary Fig. 1 A, B. For qRT-PCR, either unfed, 1-, 3-, 5-day-fed, or fully engorged *I. ricinus* females were dissected. At each time point, RNA was extracted from ten synganglia using Trizol reagent (Invitrogen), and from six pairs of salivary glands using the RNA micro kit (Qiagen). Reverse transcription was performed with Superscript III (Invitrogen) for salivary glands and the Transcriptor High-Fidelity cDNA Synthesis Kit (Roche) was used with synganglia RNA. qRT-PCR was performed using SYBR premix Ex Taq (Roche) in five and three biological replicates for synganglia and salivary glands, respectively, in a LightCycler 480 II (Roche) or a QuantStudio 6 Flex RT-PCR system (Applied Biosystems). The amplicons of *sifa_r2* in the qRT-PCR were verified by melting curves (Supplementary Fig. 1 C). The ribosomal protein S4 was used as a reference gene (Koči et al., 2013). The relative mRNA level was quantified using the ΔΔCt method, and expressed as a fold difference (Livak and Schmittgen, 2001). ΔΔCt values were calculated in Microsoft Excel and final graphs and two tailed *t*-test statistics were obtained using GraphPad Prism 5 (GraphPad Software, La Jolla California, USA).

2.6. Wholemount immunohistochemistry

For wholemount immunohistochemistry we followed our previously validated protocols for tick tissue described by Šimo et al. (2009a). Briefly, *I. ricinus* synganglia and salivary glands were dissected from either unfed or partially-fed *I. ricinus* females in phosphate buffered saline (PBS; 137 mM NaCl, 1.45 mM NaH_2PO_4, 20.5 mM Na_2HPO_4, pH 7.2) and fixed with 4% paraformaldehyde for 2 h at room temperature (RT), then washed with PBS + 0.5% Triton X-100 (PBST). Tissues were incubated with an anti-*I. ricinus/I. scapularis* SIFa_R2 affinity-purified anti-guinea pig antibody. Antibody was generated for this study by immunizing the guinea pig with an antigen targeting an epitope (C-SNTRTSMTAGRRKDSRMSD) on the carboxy-terminus of the *I. ricinus* SIFa_R2 linked to keyhole limpet hemocyanin, followed by affinity purification (Lifetein, USA). After washes in PBST, the specimens were incubated for 2 day at 4 °C with goat anti-guinea pig 488 Alexa-conjugated secondary antibodies (Life Technologies) diluted at 1:1000. For double staining, samples were incubated with a mixture of polyclonal anti-rabbit anti-SIFamide antibody (Terhzaz et al., 2007) and anti-*I. ricinus/I. scapularis* SIFa_R2, then followed by incubation with a mixture of goat anti-rabbit 594 Alexa-conjugated and goat anti-guinea pig 488 Alexa-conjugated secondary antibodies (Life Technologies). Negative controls included pre-adsorption of SIFa_R2 antibody with its corresponding antigen. Specifically, antibody was incubated with 250 μg/ml of antigen for 24 h at 4 °C and was then used for immunohistochemistry as described above. Another negative control comprised a substitution of SIFa_R2 antibody with respective guinea pig pre-immune serum (Supplementary Figs. 2 and 3). The specificity of SIFa_R2 antibody was also characterized by immunostaining in CHO cells transfected

with *sifa_r2* followed by positive and negative controls as described above. To exclude any possible cross reactivity of anti-SIFa_R2 and anti-SIFa_R1 antibodies, CHO cells transfected either with *sifa_r1* or *sifa_r2* were used for immunocytochemistry (Supplementary Fig. 4).

Samples were incubated with DAPI before mounting in Prolong Antifade Diamond Mountant (Life Technologies) and analyzed by inverted confocal microscopy using a Leica DMI8 with a z-stack tool. Assembled z-stacks were adjusted in Adobe Photoshop version 24.0.1 (Adobe Inc.). For *I. ricinus* synganglion neuronal cells, nomenclature was used as per (Šimo et al., 2009a).

2.7. Immunogold labeling

Salivary glands were isolated from unfed female *I. ricinus* and fixed in 4% formaldehyde with 0.1% glutaraldehyde in 0.1 M HEPES for 1 h at RT. After washing in HEPES buffer, specimens were embedded in 15% gelatin, cryoprotected in 2.3 M sucrose for 72 h at 4 °C before plunging into liquid nitrogen. Ultrathin cryosections were cut at −100 °C, and picked up with 1.15 M sucrose/1% methylcellulose solution (25 cp, Sigma). Sections were incubated for 1 h at RT in 1% fish skin gelatin (FSG) and labeled with an anti-guinea pig SIFa_R2 antibody diluted 1:40 in FSG for 1 h at RT. Control sections were incubated with guinea pig pre-immune serum. After washing in FSG, the sections were incubated with anti-guinea pig IgG coupled with 5 nm gold nanoparticles (BBI) diluted 1:40 in FSG for 1 h at RT. Sections were washed in HEPES, postfixed for 5 min in 1% glutaraldehyde diluted in 0.1 M HEPES, washed in dH_2O, and then contrasted/embedded using a mixture of 2% methylcellulose and 3% aq. uranyl acetate solution (9:1). Samples were observed using a JEOL 1400 TEM.

3. Results

3.1. Phylogenetic and sequence analyses of SIFa_R2

Using sequences extracted from the recent study by (Veenstra, 2021), homology searches of available databases confirmed the presence of both SIFa_R1 and SIFa_R2 in various invertebrate taxa. Phylogenetic analyses of these sequences showed two clear orthologous clusters, each containing either SIFa_R1 or SIFa_R2 proteins (Fig. 1A). Both type 1 and 2 SIFa_Rs from five different tick species (*I. ricinus*, *I. scapularis*, *Dermacentor silvarum*, *Rhipicephalus sanguineus*, and *Rhipicephalus microplus*) were also divided into these two distinct clusters.

The *sifa_r2* ORF from *I. scapularis* consists of three exons (445 bp, 102 bp, and 772 bp) interrupted by two introns (~51,340 bp and 9679 bp) (Fig. 1B). The *I. scapularis* SIFa_R1 and SIFa_R2 proteins are composed of 400 and 422 amino acid residues, respectively (Supplementary Fig. 5). Other than the incomplete sequences of SIFa_R1 from *R. sanguineus* and SIFa_R1 and SIFa_R2 from *R. microplus* at their N-terminals, all tick SIFa_R sequences contained typical motifs for seven transmembrane alpha-helical structures (Fig. 1C and Supplementary Fig. 5). The evolutionarily conserved E/DRY/F motif in the C-terminal region of the third transmembrane domain, that is typical for class A GPCRs (Calkins et al., 2019), showed differences among SIFa_R1 and SIFa_R2 protein sequences. Specifically, the SIFa_R1 sequence of all five tick species analyzed possessed an unconventional conserved DRC motif, while a conventional DRF motif was found in the SIFa_R1 sequences of all other arthropods. On the other hand, a DRY/F motif was common in tick SIFa_R2 sequences, while DRA, ERW, or ERC motifs were identified in other arthropods (Supplementary Fig. 6). The predicted SIFa_R2 protein sequence (XP_029828900) from the *I. scapularis* genome contig (DS784791) shared 98.8% identity with SIF_R2 from *I. ricinus* (GeneBank accession number BK061563) (Supplementary Fig. 7). The sequence identity of two SIFa_R paralogs from four hard tick species was between 42 and 44%, and when strongly similar amino acid residues

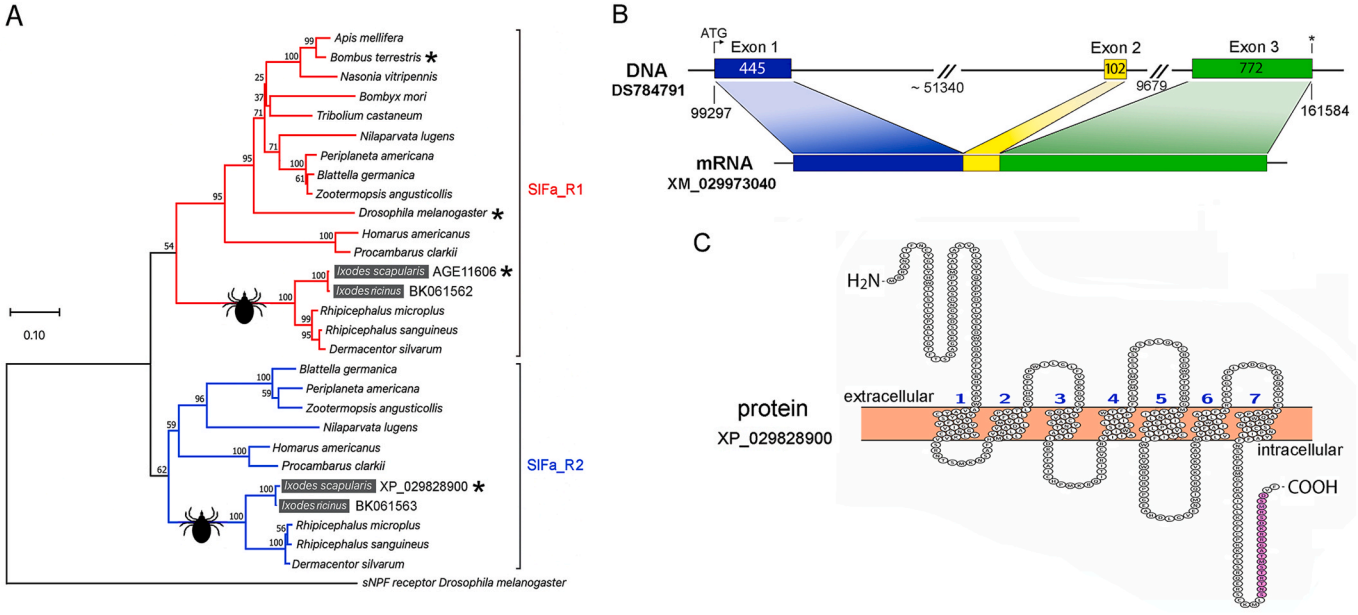

Fig. 1. (A) Phylogenetic relationships between SIFa_Rs from multiple arthropod taxa, including five tick species. Asterisks indicate deorphanized receptors. (B) Genomic organization of the *I. scapularis sifa_r2* ORF (scaffold DS784791 in scale). Three different exons are shown colored in blue, yellow, and light green, and the horizontal black lines represent introns. The numbers indicate base pair counts for either exons or introns. The ATG and the asterisk indicate the positions of the initiation and stop codons, respectively. An initial representation was generated using the Exon–Intron Graphic Marker version 4 followed by manual corrections in Adobe Photoshop. The lower part of the image illustrates a mRNA (XM_029973040) schematic of *sifa_r2* indicating the proportional length of the exons. (C) Schematic representation of SIFa_R2 protein (XP_029828900) transmembrane organization using Protter 1.0 software. Blue numbers show transmembrane helices, and pink highlights the epitope targeted by the anti-SIFa_R2 antibody in this study. GenBank accession numbers of all sequences used are listed in the Supplementary spreadsheet.

were taken into account, similarity reached 62–65% (Supplementary Fig. 5).

3.2. Ligand-receptor interactions

The *I. scapularis* SIFamide showed robust dose-dependent luminescent responses with an EC_{50} value of 6.8 nM when interacting with the heterologously expressed *I. scapularis* SIFa_R2 (Fig. 2A). Higher concentrations of SIFamide peaked luminescence within the first 3 s, while the lower concentration triggered responses within 4–8 s after ligand application (Fig. 2B). Insect SMYamide peptides such as *M. extradentata* GMYamide, *L. migratoria* AMYamide, and *B. germanica* SMYamide activated the receptor with EC_{50} values of 7.9 nM, 58.2 nM, and 150.5 nM, respectively. IMFamide from *B. mori* did not show any significant activation of *I. scapularis* SIFa_R2 (Fig. 2A, D). We also investigated whether the previously identified *I. scapularis* SIFa_R1 (Šimo et al., 2013) could also be activated by insect SMYamides and *B. mori* IMFamide. SIFa_R1 exclusively interacted with SIFamide with an EC_{50} value of 326.9 nM, and no or extremely low responses were detected with insect SMYamides or *B. mori* IMFamide (Fig. 2C, D, E). In the case of SIFa_R2, the specificity of the expressed receptors was confirmed by a lack of luminescent response in mock transfected cells. In addition, the other tested neuropeptides did not activate SIFa_R2 (for all the ligands tested see section 2.3. Functional receptor assays).

3.3. I. scapularis SIFa_Rs bind the C-terminus of amidated peptides

Peptide terminal orientation within the *I. scapularis* SIFa_R binding cavity was determined by homology modeling and chemistry assessment of GPCR peptide-binding residues (Fig. 3A and Supplementary Fig. 8). The class A GPCR, human Ox2R, was used as a template to construct both SIFa_R protein models. Based on multiple sequence alignments from remote homologs, the Phyre2 server (Kelley et al., 2015) also confirmed Ox2R as ~36% similar to both *I. scapularis* SIFa_R primary sequences. Among the 25 GPCR peptide-binding residues, 5 Ox2R residues were conserved in both SIFa_Rs (Fig. 3A). Particularly conserved was SIFa_R1 $Q142^{3.32}$ and SIFa_R2 $Q164^{3.32}$ that interact with the amidated C-terminus of peptides. An additional 5 out of 25 conserved positions between the SIFa_Rs were also identified among class A GPCRs that bind amidated C-terminal peptides. Eight positions were expressed by both C- and N-terminal peptide-binding GPCRs. Two substitutions expressed by SIFa_R2 ($H145^{2.65}$ and $E345^{7.32}$) were juxtaposed with two Ox2R peptide-binding residues ($D115^{2.65}$ and $H224^{5.39}$). These respective *I. scapularis* residue positions were polar ($N123^{2.65}$) and non-polar ($L320^{7.32}$) in SIFa_R1. The remaining 5 GPCR peptide-binding residue positions were polar substitutions in SIFa_R1 and non-polar in SIFa_R2 (Fig. 3A).

The low N-terminus primary sequence conservation between arthropod SIFa_R1s and SIFa_R2s (Supplementary Fig. 5) is represented by the lack of protein secondary structures (e.g., α-helices and/or β-sheets) for both *I. scapularis* SIFa_R N-termini (Fig. 3B and Supplementary Fig. 8). The TM domains, however, are highly resolved with an α-carbon backbone root mean square deviation (RMSD) of 2.5 Å (SIFa_R1) and 2.4 Å (SIFa_R2) compared to the peptide-bound Ox2R (PDB: 7L1U) (Hong et al., 2021). After MD refinement within a POPC lipid bilayer, the *in-silico* bound complexes depicted the SIFamide peptide C-terminus as oriented towards the *I. scapularis* SIFa_R2 cavity (i.e., Fig. 3B). The bound complexes were analyzed with PDBePISA (Krissinel and Henrick, 2007) to detect initial peptide residue(s) forming contacts with the distinct *I. scapularis* SIFa_R2 residue positions, $H^{2.65}/E^{7.32}$, and/or the SIFa_R1 substitutions, $N^{2.65}/L^{7.32}$ (Fig. 3A). The backbone of the non-polar SIFamide peptide residue, F7, interacted with the polar

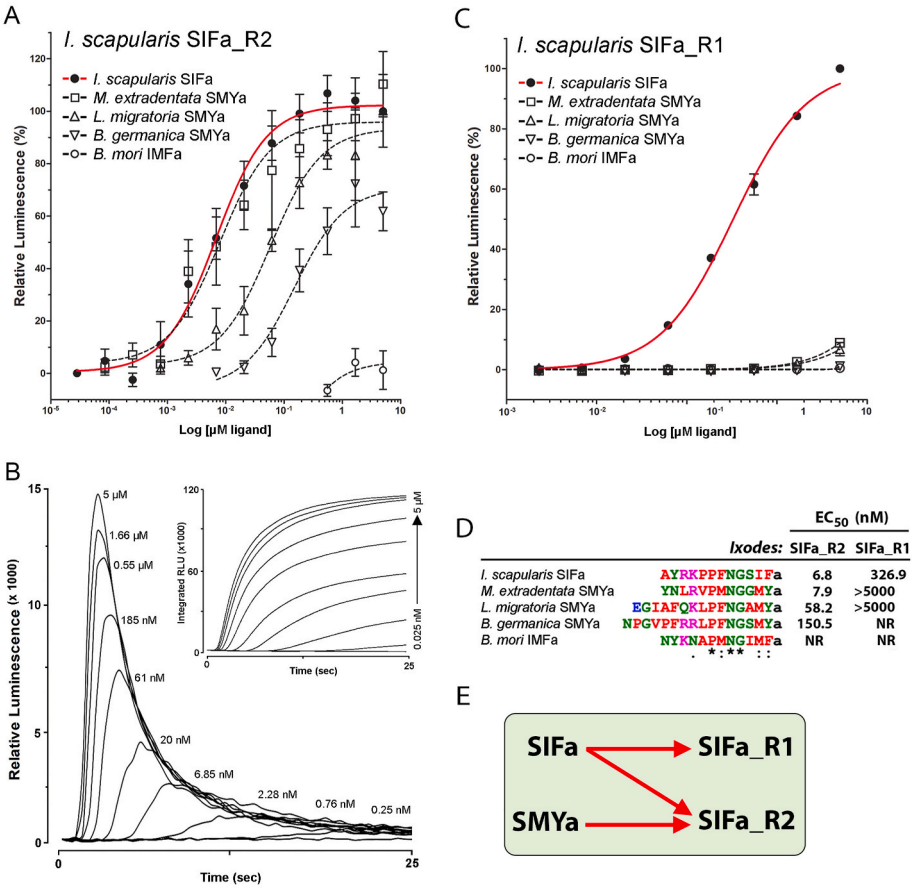

Fig. 2. Bioluminescent aequorin-based functional assays of *I. scapularis* SIFa_R2 and SIFa_R1 in CHO–K1 cells. (A) Dose-response curves for SIFa_R2 against SIFamide (red line) and its insect paralogs (dotted lines). (B) Typical 25 s cellular responses of SIFamide-mediated calcium mobilization via SIFa_R2 expressed by CHO–K1 cells. The inset in B shows integrated values from 0.025 nM–5 µM SIFamide concentrations. (C) The dose-response curves for SIFa_R1 against the same ligands as used in (A). (D) EC_{50} (nM) of different ligands on two different *I. scapularis* SIFamide receptors. Peptide sequences are given and the colors of the letters highlight the physicochemical properties of peptide amino acid residues; small hydrophobic (red), acidic (blue), basic (magenta), and hydroxyl + sulfhydryl + amine + G (green). Asterisks indicate identical amino acid residues, colons indicate amino acids with strongly similar properties, and periods indicate amino acids with weakly similar properties. Note that no response (NR) for either SIFa_R1 or SIFa_R2 was detected with *B. mori* IMFamide. (E) A proposed schema depicting the interactions of SIFamide and SMYamide with two different SIFa_Rs. The bars in A and C indicate the standard error for a minimum of three biological replications. In A and C panels, some standard error bars are smaller than the symbols used and, in these cases, only the symbols are shown.

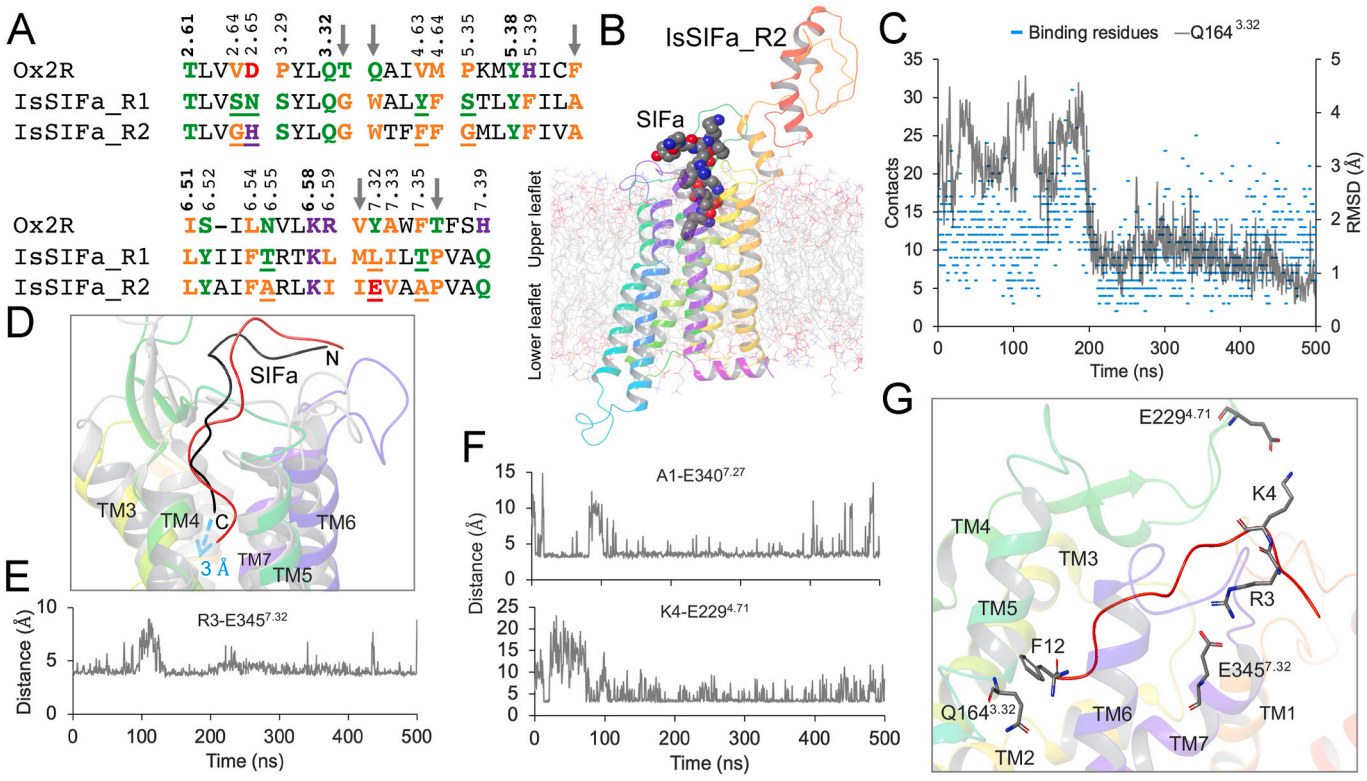

Fig. 3. (A) The 25 class A GPCR binding site residue positions are numbered and colored in bold as non-polar (orange), polar (green), acidic (red), and basic (purple). Bold alignment positions (top) are conserved/similar residues. Arrows indicate residues found among GPCRs binding peptides at the amidated C-terminus (Tikhonova et al., 2019). Underlined residues indicate different chemistry between the *I. scapularis* SIFa_Rs (IsSIFa_R) and Ox2R – the human orexin type 2 receptor. These 25 SIFa_R2 binding site residue positions are also indicated in Supplementary Fig. 5 as asterisks and underlined with neighboring residues in Supplementary Fig. 8. (B) The MD refined, peptide bound [atoms as spheres: carbon (grey), nitrogen (blue), and oxygen (red)], *I. scapularis* SIFa_R2 predicted structure. Color-coded from the N-terminus (red) to the C-terminus (purple) and embedded in a POPC bilayer with leaflets indicated. Hydrogen atoms, water molecules, and ions are not shown. (C) The contacts formed (y-axis; cyan dashes) 25 between the *I. scapularis* SIFa_R2 binding residues (color-coded in panel A) and the entire SIFamide peptide during the 500 ns MD (x-axis). The secondary y-axis is the root mean square deviation (RMSD) of SIFa_R2 residue Q164$^{3.32}$. (D) The *I. scapularis* SIFa_R2 starting (grey) and end conformations after 500 ns MD (color-coded as in 'B') with labeled peptide termini (N and C) and GPCR TMs. The distance between the SIFamide C-terminus starting (black) and end conformations (red) is indicated. (E–F) The terminal sidechain carbon distances (y-axis) between interacting residues of SIFamide peptide and *I. scapularis* SIFa_R2 (legend) during 500 ns MD (x-axis). (G) The *I. scapularis* SIFa_R2 MD end conformation (TMs labeled) with noteworthy residue interactions shown.

sidechain of SIFa_R1, N123$^{2.65}$ (Supplementary Fig. 9A). Noteworthy are the potential electrostatic interactions between the SIFa_R2 E345$^{7.32}$ with the SIFamide peptide residue, R3. These respective sidechain oxygen (E345$^{7.32}$) and nitrogen (R3) atoms were approximately ~3.6 Å (Supplementary Fig. 9B). There were no initial SIFamide peptide interactions detected regarding SIFa_R1 L320$^{7.32}$ or SIFa_R2 H145$^{2.65}$.

A 500 ns MD simulation was subsequently conducted to determine the *in-silico* stability of *I. scapularis* SIFa_R2-peptide interactions. In total, 15 out of 25 SIFa_R2 binding residues maintained interactions with the SIFamide peptide (Supplementary Fig. 9C). These peptide-GPCR residue interactions peaked and suddenly dropped approximating 200 ns (cyan dashes in Fig. 3C). This binding flux coincided with a high sidechain motion of the SIFa_R2 residue, Q164$^{3.32}$ (grey line in Fig. 3C). After 200 ns, the reduced peptide-GPCR interactions conformed during the equilibration of Q164$^{3.32}$ deviation (Fig. 3C). Moreover, the Q164$^{3.32}$ residue maintained its contacts with the peptide amidated C-terminal residue, F12, for 30% of the MD (Supplementary Fig. 9C). The apparent sidechain motion shift and equilibration of SIFa_R2 Q164$^{3.32}$ (Fig. 3C) was caused by the repositioning of the SIFamide peptide, as denoted by a 3.0 Å C-terminal deviation between the MD conformations (Fig. 3D). The α-carbon backbone RMSD for the TM domains between the starting and end MD conformation was 2.9 Å.

A prominent interaction that was strongly maintained throughout the 500 ns MD (Supplementary Fig. 9C) was between the SIFamide peptide residue R3 and the *I. scapularis* SIFa_R2 residue E345$^{7.32}$ (Fig. 3E). Additional contact analysis between the entire complex detected highly maintained interactions (i.e., >50% of the MD simulation) for peptide-SIFa_R2 residues, A1-E340$^{7.27}$ and K4-E229$^{4.71}$ (Fig. 3F). The SIFa_R2 negative residues, E229$^{4.71}$and E345$^{7.32}$, structurally opposed one another, causing an electrostatic "tunnel" for the N-terminal positive SIFamide residues, R3 – K4 (Fig. 3G). Given the proximity and interactions of the peptide amidated C-terminal residue, F12, and the SIFa_R2 Q164$^{3.32}$ (Fig. 3G and Supplementary Fig. 9C), the Q164$^{3.32}$ equilibration shift during the MD simulation (Fig. 3C–D) was potentially caused by the strongly maintained interactions of R3-E345$^{7.32}$ and K4-E229$^{4.71}$ (Fig. 3E–G).

3.4. The spatial and temporal expression of *sifa_r2* in salivary glands and synganglia

Tissue-specific RT-PCR of four-day-fed *I. ricinus* females revealed expression of *sifa_r2* in salivary glands, synganglia, midguts (including hindguts), trachea, ovaries, and carcasses, but not in the Malpighian tubules (Fig. 4A).

Quantitative RT-PCR of *sifa_r2* in *I. ricinus* salivary glands demonstrated the presence of the transcript in unfed females with an approximate 70% decrease during the feeding period (days 1, 3, and 5 of feeding). The mean transcript values were lower in replete females and represented an approximate 80% drop compared to the levels obtained in salivary glands at the unfed stage (Fig. 4B). In synganglia, relative

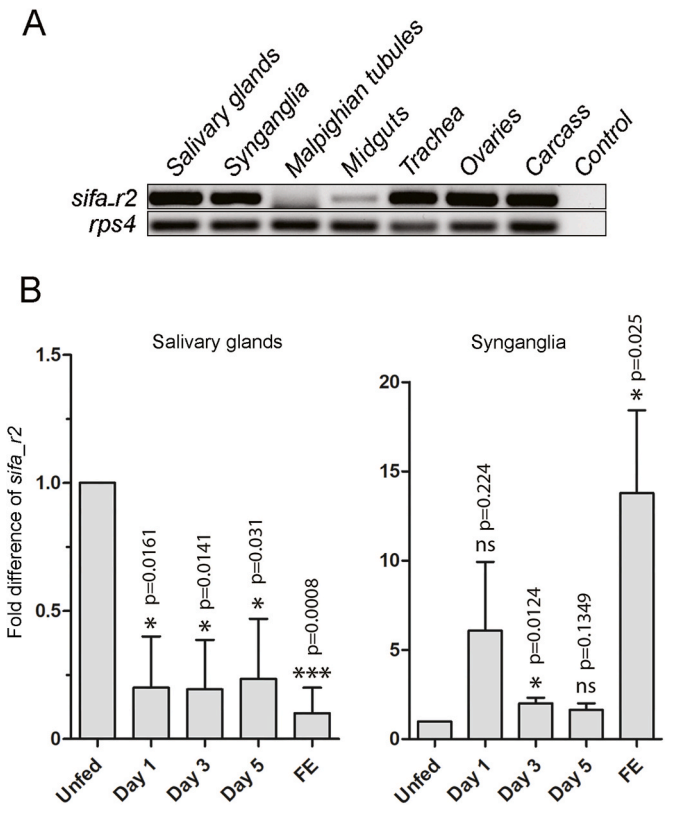

Fig. 4. (A) Tissue-specific RT-PCR of *sifa_r2* in different tissues from partially-fed *I. ricinus* females compared to *rps4* ribosomal protein S4 transcript. Note that midguts represent both the midguts and hindguts, and for the control, no DNA template was added to the PCR reaction. Full-length gels including amplicon sizes can be found in Supplementary Fig. 10. (B) Fluctuations of the *sifa_r2* mRNA in unfed and feeding *I. ricinus* females. The bars in panel B indicate the standard error for three and five biological replicates of salivary glands and synganglia, respectively. Asterisks indicate the comparison of the mean to the value of the unfed stage using a one-way Student's t-test ($P \leq 0.05$). Data were normalized using the ribosomal protein S4 (RPS4) transcript, and the expression levels in unfed ticks were assigned a value of 1. FE – fully engorged, ns – not significant.

sifa_r2 levels during the feeding stages were slightly elevated compared to the unfed stage. However, a significant increase (~15 fold) was detected in fully engorged females that dropped from the host (Fig. 4B). Given the close relationship between *I. scapularis* and *I. ricinus* species, we propose that the gene expression data are applicable to both tick species.

3.5. Immunostaining of SIFa_R2 in salivary glands and synganglion

Positive anti-SIFa_R2 antibody immunoreactivity (IR) was detected exclusively in the basal regions of both type II and III acini from *I. ricinus* females (Figs. 5–8, Video 1 and 2).

Supplementary video related to this article can be found at https://doi.org/10.1016/j.ibmb.2023.103963

Specifically, in type II acini of unfed females, wholemount immunohistochemistry revealed robust IR in the cytoplasm and likely within the cell membranes of basally located acinar cells (Fig. 5A–C, Video 1). In-depth immunolabeling at the ultrastructural/electron microscopy level confirmed SIFa_R2 presence in three cellular types within the acinar basal region surrounding the acinar duct: single MC, ECs, and large basal granular cells (GCs) (Fig. 5E–K). Immunoreactivity on ECs and the MC was observed in close proximity to the single large-caliber electron-dense axon and the single smaller-caliber electron-lucent axon, that were surrounded by convoluted membranes of ECs and the MC (Fig. 5E–G, I, K). Basal GCs were positive in the region adjacent to the acinar duct (Fig. 5E, H). Interestingly, the large basal axon containing electron-dense vesicles was also positive for SIFa_R2 immunogold labeling (Fig. 5 F, K).

In type III acini of unfed females, wholemount IHC revealed a strong signal in the region just above the apical side of the acinar valve, extending basally along the acinar duct (Fig. 6 A-C, Video 2). Immunogold labeling of the basal acinar region confirmed the reaction in the MC (Fig. 6D–F) and in basal GCs with large nuclei (Fig. 6G–J). At the region above the acinar valve, the IR in GCs was observed in extremely close proximity to the large electron-dense axon (Fig. 6 J, K). The axolemma of this axon was also positive with anti-SIFa_R2 antibody (Fig. 6K).

Double staining for SIFa_R2 and SIFamide in salivary glands from four-day-fed *I. ricinus* females, clearly showed that SIFa_R2-IR was present in the cytoplasmic region of six basal GCs in close proximity to SIFamide-immunoreactive axon terminals (Fig. 7). Here, a strong reaction was observed with the SIFa_R2 antibody in vesicles, presumably endomembranes belonging to the Golgi complex and/or endoplasmic reticulum (ER) (Fig. 7A–C). Interestingly, a similar staining pattern was also observed during the heterologous expression of *sifa_r2* in CHO cells (Supplementary Fig. 4). No reaction with SIFa_R2 antibody was observed in type II acini from four-day-fed females. A schematic drawing (Fig. 8) summarizes all SIFa_R2 immunoreactions in salivary gland acini from unfed and partially-fed females.

In unfed *I. ricinus* females, the anti-SIFa_R2 antibody recognized nine pairs of neurons in different regions of the synganglion. In the dorsal protocerebrum one pair of lateral (PcDL) and three pairs of medial neurons ($PcDM_{1\text{-}3}$) were detected, while on the ventral side, a single pair of small medial neurons (PcVM) was detected (Fig. 9 A, B and D). In the first pedal lobes, two dorsal neurons (Pd_1DM) were found in close proximity to the esophagus (Fig. 9 A, C). In the opistosomal lobe, a pair of dorsal medial (OsDM) and two pairs of ventral medial ($OsVM_{1,2}$) neurons were identified (Fig. 9 A, C and D).

4. Discussion

Here, we deorphanized the *I. scapularis* GPCR protein XP_029828900 and proved its high biological affinity to the SIFamide ligand, thus we consider it to be a second SIFa_R in the genome of this tick species. We identified the first *I. scapularis* SIFa_R1 in our previous study (Šimo et al., 2013), and when taken in tandem with the current results, *I. scapularis* is the first arthropod species in which two different SIFa_Rs have been functionally characterized. Phylogenetic analysis revealed that the two SIFa_Rs are conserved in the tick lineage and possess a moderate level of similarity (~65%) within this particular species. The impressively high level of SIFa_R2 protein identity (98.8%) between *I. ricinus* and *I. scapularis* supports the allopatric relationship of these two hard tick species. The identification of a DRC motif in the intracellular extension of the third transmembrane domain of SIFa_R1 exclusively within the tick lineage is a new finding. These highly conserved three-amino acid residues are well known for their role in GPCR conformation and G protein recognition. In functionally characterized tick GPCRs such as kinin, pyrokinin, or periviscerokinin, a common DRY or ERY motif is featured (Holmes et al., 2000, 2003; Yang and Zhang, 2015; Yang et al., 2013), while variations in this motif were assigned to the functional differentiation of allatoregulatory peptides and their receptors in insects (Verlinden et al., 2015). Thus, the new DRC motifs in tick SIFa_R1 may be associated with specific physiological role(s) in the tick salivary gland.

The existence of two different SIFa_Rs in some arthropod taxa was first suggested by an *in silico* study, leading to a hypothesis that in species lacking a SIFamide neuropeptide paralog in their genomes, that SIFamide was the only authentic ligand for both of these receptors (Veenstra, 2021). This appears to be true in ticks, where only the SIFamide neuropeptide and two SIFamide-sensitive receptors have been identified

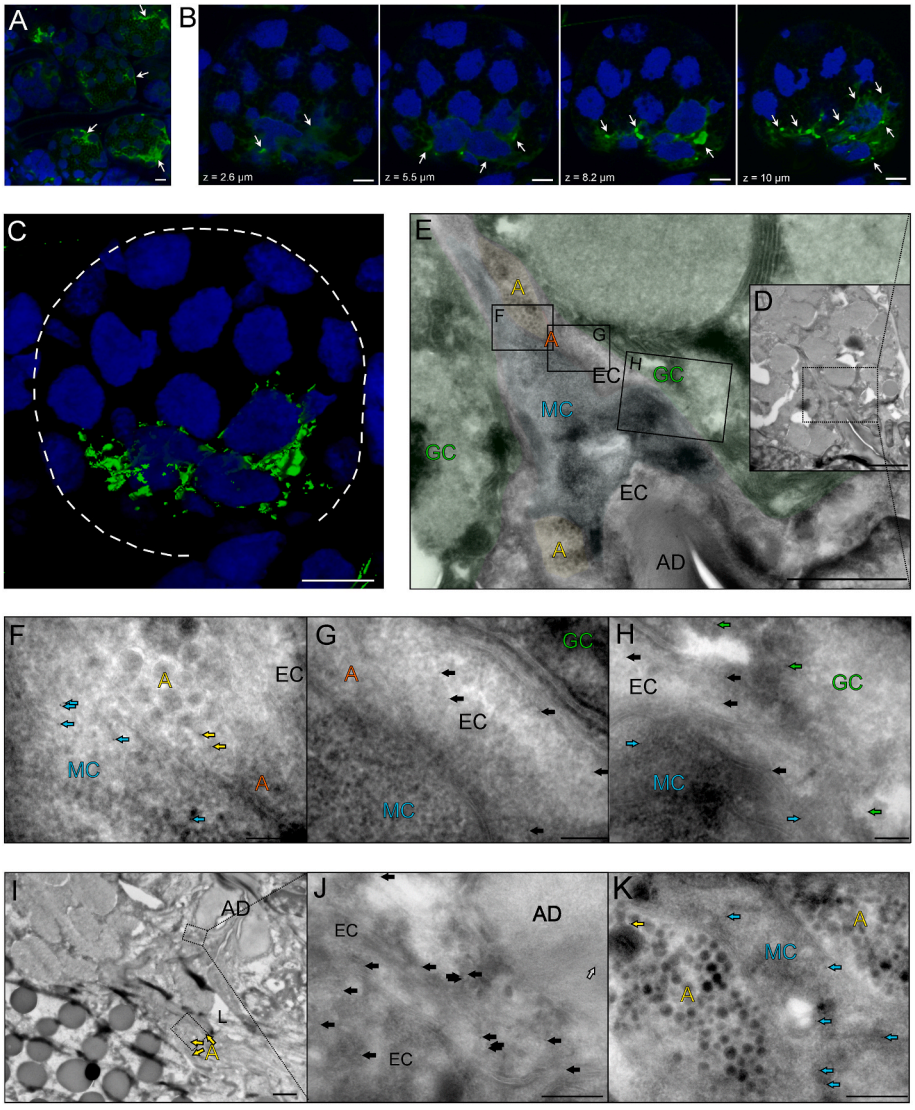

Fig. 5. Immunolocalization of SIFa_R2 in unfed *I. ricinus* female salivary gland type II acini. (A–C) Wholemount immunohistochemistry. (A) Multiple type II acini showing immunoreactivity with anti-SIFa_R2 antibody at basal regions (green, arrows). (B) Z-stack image series of single type II acinus highlighting the immunoreactive basal region (green, arrows). (C) Surface-rendered model of 3D reconstruction of confocal z-stack images (from B). The dotted line indicates the acinus boundary. The 3D movie of image C is available in Supplementary Video 1. (D–K) Transmission electron microscopy image showing immunogold labeling of SIFa_R2 (5 nm nanoparticles) in type II acinus. (D–H) Labeling of SIFa_R2 in the basal region surrounding the acinar duct (AD). The greenish color in E distinguishes the basal granular cells (GCs). The inset in D is magnified in E-H. In F through K, positive immunoreactivity in different cell types is shown as follows: black arrows – basal epithelial cells (ECs), aqua blue arrows – myoepithelial cell (MC), green arrows – GCs, yellow arrows – axons with electron-dense neurosecretory vesicles (yellow letter A). Note that only this type of axon (yellow A) demonstrated positive SIFa_R2 staining (yellow arrows in F and K), while axons with the electron-lucent vesicles (orange letter A) did not (F, G). (I–K) Immunoreactivity in ECs (black arrows), MCs (aqua blue arrows), and axons with electron-dense vesicles (yellow letter A, yellow arrows) in the region above the acinar valve magnified in (J) and in the region close to the acinar lumen (letter L) magnified in (K). Blue in A-C is DAPI staining for nuclei. Scale bars are 10 µm (A–C), 5 µm (D), 2 µm (E, I), 200 nm (F–H, J), and 500 nm (K). For a simpler rendering see the schematic drawing in Fig. 8.

(this study and Šimo et al., 2013). Moreover, Veenstra (2021) also suggested that insect SIFamide neuropeptide paralogs with unidentified receptor(s) could be potential ligands for one or both SIFa_R types. While there is no evidence that SIFamide paralogs exist in the tick lineage, we tested if paralogs of this neuropeptide from four different insect species could activate *I. scapularis* SIFa_R2. We experimentally proved the high biological affinity of various insect SMYamides to *I. scapularis* SIFa_R2, supporting the hypothesis that in addition to SIFamide, SIFa_R2 is an authentic receptor for SIFamide paralogs in certain arthropod taxa. Interestingly, *I. scapularis* SIFa_R1 was exclusively responsive to the SIFamide ligand, while SMYamides failed to activate the receptor. Therefore, we suggest that both SIFa_R types are authentic receptors for SIFamide, whereas only SIFa_R2 is also sensitive to SIFamide paralogs. In species harboring both types of ligands along with both receptors, it would be interesting to investigate whether SIFa_R2 is a target for SIFamide and/or SMYamide in specific tissues. The "message-address" hypothesis for GPCR-peptide binding designed by Schwyzer (1977) was used to describe Ox2R-peptide interactions (Hong et al., 2021). This hypothesis states that the peptide N-terminus is crucial in GPCR activation, e.g., the "message", and the peptide C-terminus enhances receptor activation for downstream signaling, e.g., the "address". Concurrently, the positive N-terminal SIFamide residue positions, R3-K4, may act as the "message" by forming initial electrostatic interactions with SIFa_R2 E229$^{4.71}$and E345$^{7.32}$. The interactions between the SIFamide amidated peptide C-terminal residue, F12, and the SIFa_R2 Q164$^{3.32}$, therefore, act as the "address" during cell signaling. Follow-up mutation studies should focus on the positive N-terminal SIFamide and SMYamides residue positions and/or SIFa_R2 E229$^{4.71}$ and E345$^{7.32}$. Interestingly, an SIFamide paralog from *B. mori*, an IMFamide (Roller et al., 2008)—demonstrating greater sequence differences to SIFamide than SMYamides to SIFamide (Veenstra, 2021)—did not activate the *I. scapularis* SIFa_R2, nor the SIFa_R1. While it seems that *Bombyx* only possesses SIFa_R1 (Veenstra, 2021) in the genome, it is likely that IMFamide may act via an as-yet unidentified receptor.

Despite the high nucleotide sequence identity among *I. ricinus sifa_r1* and *sifa_r2* ORFs, the *sifa_r2*-specific amplification allowed us to investigate the spatial and temporal expression of this transcript as well as to compare it with the expression profile of the previously identified *sifa_r1* (Šimo et al., 2013). The spatial mapping of *I. ricinus sifa_r2* expression revealed its presence in various tick organs including salivary glands and synganglia. Salivary glands were suggested as a target tissue of axonal SIFamide in our previous reports (Šimo et al., 2009b, 2013). Therefore, it is not a surprise that *sifa_r2* was also detected in these tissues. The presence of *sifa_r2* in *I. ricinus* trachea, ovaries, and carcasses (ventral cuticle, legs, fat, and tissue debris), indicates that SIFamide may act as a neurohormone. Interestingly, very weak or no expression was observed in *I. ricinus* midguts and Malpighian tubules, respectively. These results

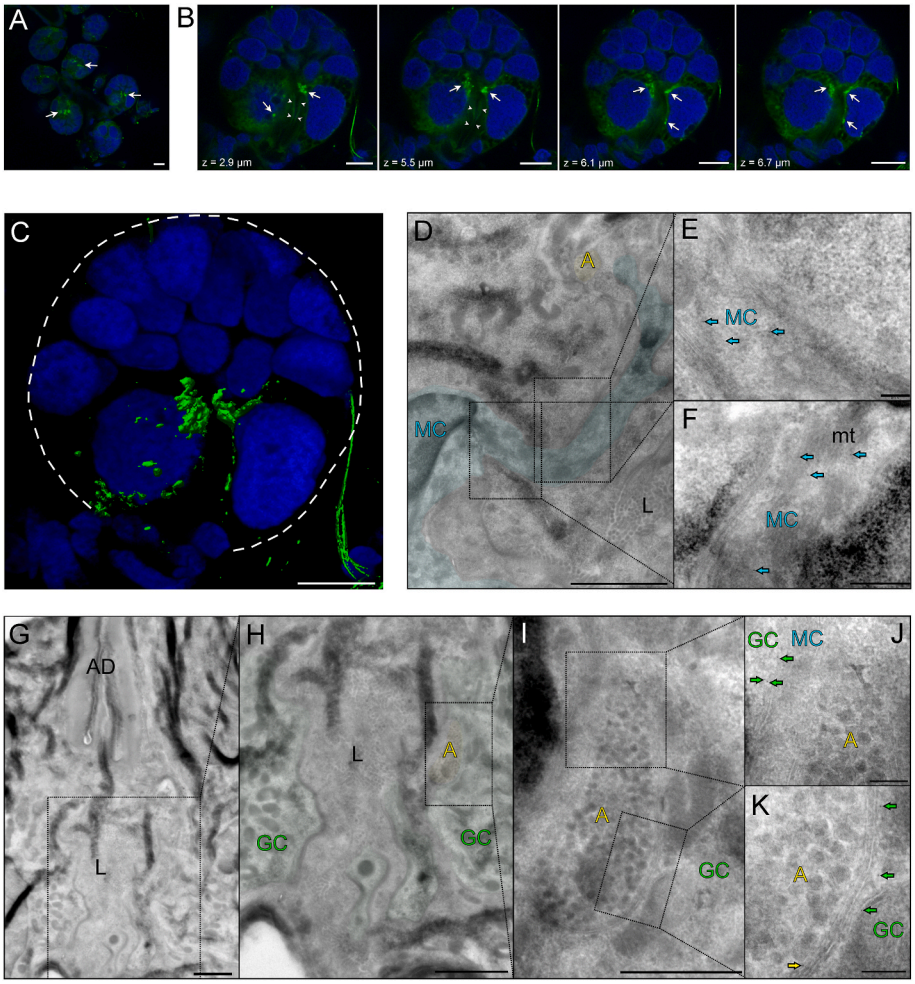

Fig. 6. Immunolocalization of SIFa_R2 in unfed *I. ricinus* female salivary gland type III acini. (A–C) Wholemount immunohistochemistry. (A) Multiple type III acini expressing SIFa_R2 at basal regions (green, arrows). (B) Z-stack image series of a single type III acinus highlighting the immunoreactivity (green, arrows). Arrowheads in (B) show the valve region of the acinar duct. (C) Surface-rendered model of 3D reconstruction of confocal z-stack images (in B). The 3D movie of image C is available in Supplementary Video 2. The dotted line indicates the acinar boundary. (D–K) Transmission electron microscopy image showing immunogold labeling (5 nm nanoparticles) of SIFa_R2 in type III acinus. (D–F) Labeling of SIFa_R2 (aqua blue arrows) in the myoepithelial cell (MC). Note that the MC is distinguished by a bluish coloration in D. Insets in D are magnified in E and F. Axons with electron-dense vesicles (yellow letter A). (G–K) In basal regions of acinus above the acinar valve, the labeling was observed in basal granular cells (GCs, green arrows) with large nuclei and in the axolemma (yellow arrow) of the axon with electron-dense vesicles (yellow letter A). Insets in G, H, and I are magnified in H, I, J, and K respectively. GCs in H are distinguished by a greenish coloration. Note that the reaction in GCs was in very close proximity to the axon (J, K). AD – acinar duct. L – acinar lumen, mt – microtubules. Blue in A-C is DAPI staining for nuclei. Scale bars are 10 µm (A–C), 2 µm (D, G, H), 200 nm (E, J, K), 500 nm (F), and 1 µm (I). For a simpler rendering see the schematic drawing in Fig. 8.

corroborate those obtained in the cockroach *Periplaneta americana* (Veenstra, 2021), suggesting convergent evolution of SIFamide signaling systems in these two arthropod species. Monitoring of *sifa_r2* temporal dynamics in salivary glands throughout feeding showed the highest level of the transcript in unfed females, which lowered approximately 0.6 fold during feeding and 0.8 fold during replete stages. We speculate that the high transcript level observed in the unfed stage, along with the robust protein immunodetection of SIFa_R2 around the acinar valve, indicate a potentially important role for the protein in unfed salivary gland physiology. Subsequently, likely due to the massive pre-synthesis in the unfed stage, the transcript level decreases during feeding, while possible slow receptor protein turnover helps maintain its continued immunodetection at this stage. In addition, two previous studies also showed that transcript levels of SIFamide neuropeptide in *I. scapularis* synganglia do not significantly increase during feeding, rather they decrease during days three to five of female feeding (Egekwu et al., 2016; Šimo et al., 2013). These observations may be consistent with the slow feeding period of *Ixodes* females, in the range from day 1 to day 5–6 of feeding, where a decreased but constant level of SIFa_R2 and its ligand perform their physiological role(s). Interestingly, a similar pattern for unfed and feeding stages was observed for *I. scapularis sifa_r1* transcript in our previous study (Šimo et al., 2013) indicating the same temporal needs of both receptors for SIFamide signaling in the salivary glands. Furthermore, a ~10- to ~15-fold increase of *sifa_r2* transcript levels in replete tick synganglia compared to feeding and unfed stages, respectively, suggests the importance of the receptor in post-feeding processes, although at this point it is difficult to predict the specific function of this receptor in the synganglion circuit. Furthermore, the distribution of neurons detected by anti-SIFa_R2 antibody appeared not to overlap with SIFa_R1 neurons described in our previous study (Šimo et al., 2013), suggesting different SIFamide receptor types exert selective control of certain neuronal cell populations.

Our immunostaining approaches confirmed the expression of SIFa_R2 on the ECs (type II acini) and the MC (type II and III acini) close to the apex of the acinar duct. This finding corresponds to results from our recent study where SIFa_R1 IR was also associated with these two cell types, both encapsulating large-caliber SIFamide axons with electron-dense neurosecretory vesicles, as well as overlying the arms of the acinar valve (Vancová et al., 2019). Thus, our current results support the assumption that synaptic SIFamide regulates the activity of the acinar valve via two different surface receptors (SIFa_R1 and SIFa_R2) expressed by ECs and the MC. In addition, SIFa_R1 was previously observed on small electron-lucent axons with unknown function, surrounding the large electron-dense SIFamide axons, both encapsulated by the MC (Vancová et al., 2019). Here, an occasional signal with SIFa_R2 antibody was found on large electron-dense axons or their axolemma. Presumably these axons correspond to SIFamide-releasing axons, and we speculate that axonal SIFa_R2 may serve here as an autoreceptor for the negative feedback loop in signal transduction, as has been shown for insect neuropeptide receptors (Choi et al., 2012).

A completely novel finding was the association of SIFa_R2 with basal GCs in both type II and III acini. Previously, we described that SIFamide axons are in occasional contact with GCs, but postsynaptic SIFa_R1 was not detected on these cells (Vancová et al., 2019). Thus, our current results have led to the assumption that SIFamide may target basal GCs via its second receptor (SIFa_R2). Although the functional significance of

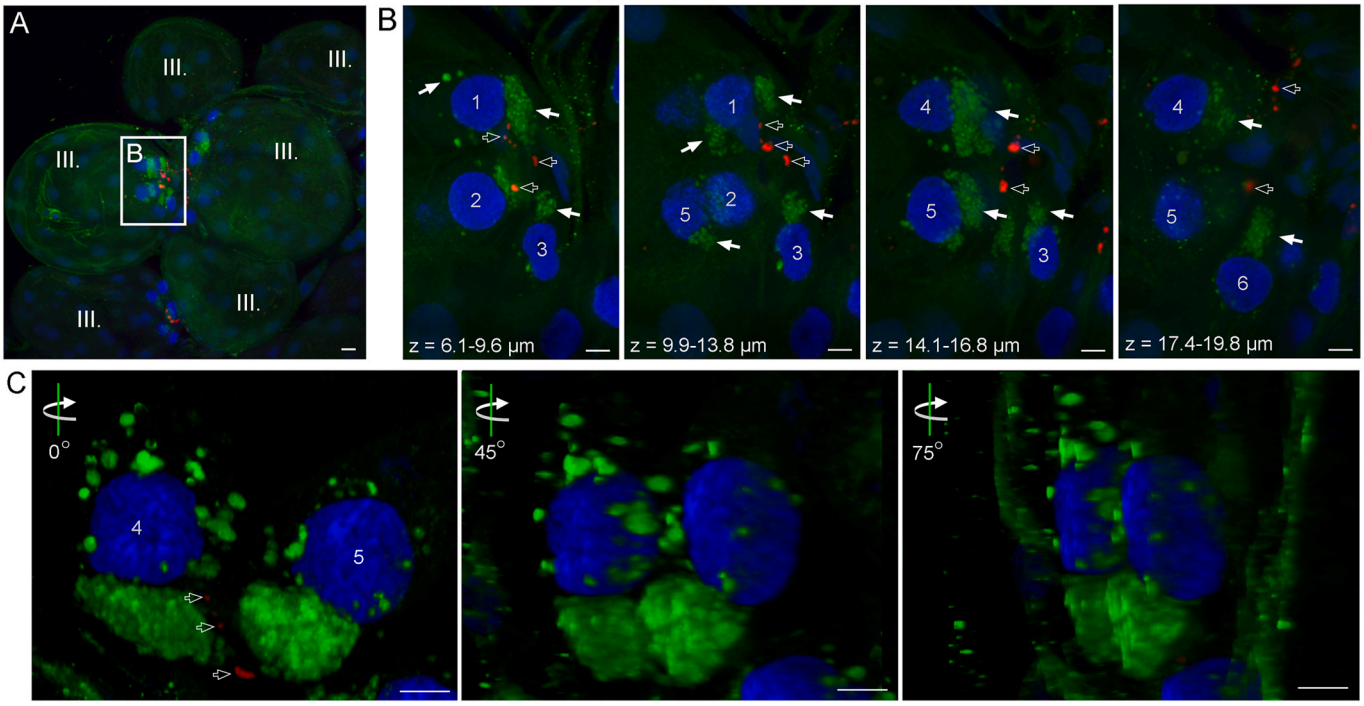

Fig. 7. Double staining of SIFa_R2 and SIFamide neuropeptide in the basal region of type III acini in four-day-fed *I. ricinus* females. (A) A merged z-stack confocal image of type III acini (Roman numeral III). (B) Z-stack image series of single type III acinus highlighting the immunoreactive basal region. Note that SIFamide-immunoreactive axon terminals (red, empty arrows) were in close proximity to the acinar basal granular cells expressing SIFa_R2 (green, arrows). Numbers (1–6) indicate specific basal granular cells. (C) A micro-rotation of the 3D-reconstructed confocal image of basal acinar cell numbers 4 and 5 (in B). The green color in C corresponds to staining with anti-SIFa_R2. Empty arrows in the first panel highlight staining with SIFamide neuropeptide (red). Blue is DAPI staining for nuclei. Scale bar is 10 µm. For a simpler rendering see the schematic drawing in Fig. 8.

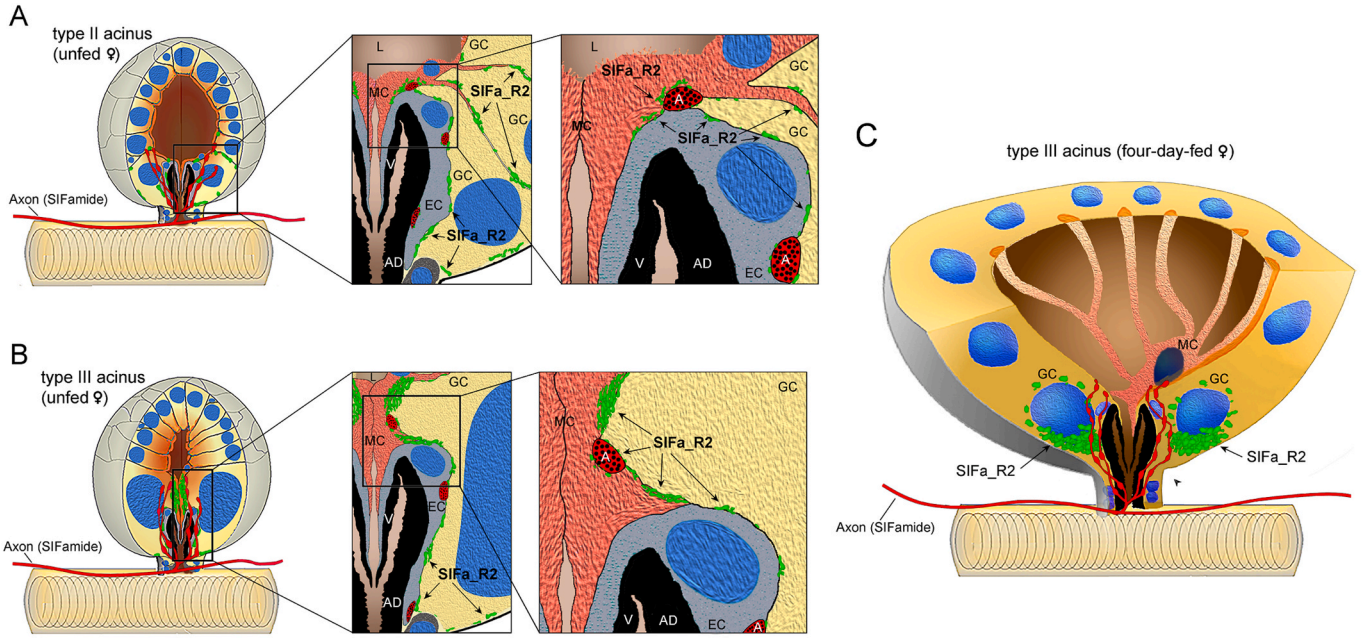

Fig. 8. A schematic representation of *I. ricinus* salivary gland type II and III acini highlighting their cellular organization and expression of SIFa_R2. The schema was reconstructed based on wholemount and TEM immunostaining approaches. (A, B) Type II and III acini of unfed female. Insets in A and B are magnified in a section-type manner. The SIFa_R2 (green) immunoreaction was commonly observed on the basal part of the myoepithelial cell (MC), basal epithelial cells (EC) and basal granular cells (GC), all in close proximity to SIFamide axon terminals (red, white letter A). (C) A basal region of a type III acinus from a four-day-fed female displaying SIFa_R2 (green). L – lumen, V – valve, AD – acinar duct. A schema displaying SIFa_R1 in *I. scapularis* salivary glands can be found in Vancová et al. (2019). The 3D schemas of acini were modified from Šimo et al. (2011, 2013).

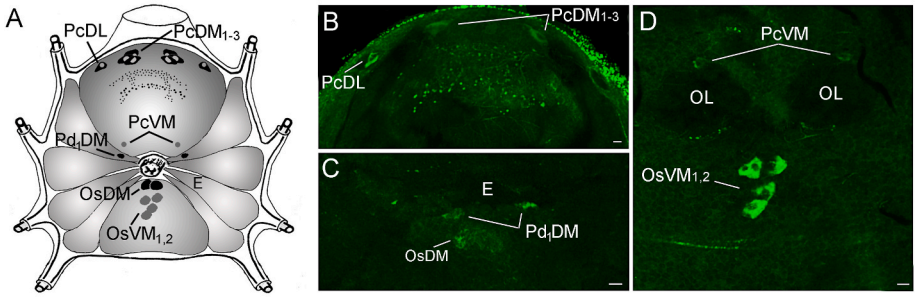

Fig. 9. Immunolocalization of SIFa_R2 in the synganglion of unfed *I. ricinus* females. (A) Schematic illustration of all neurons detected with the anti-SIFa_R2 antibody. (B) The dorsal anterior part of the synganglion. (C) The central dorsal region of the synganglion. (D) The central ventral region of the synganglion. E – esophagus, OL – olfactory lobes. For neuron nomenclature, the first two letters refer to the position of each neuron in a specific lobe of the synganglion, protocerebral (Pc), pedal 1–4 (Pd1–4), opisthosomal (Os), and the letters that follow refer to the anatomical location of the neuron: dorsal (D), ventral (V), anterior (A), posterior (P), medial (M), or lateral (L). Scale bar is 20 μm.

the observed immunoreactive SIFa_R2 in the Golgi/ER (endomembranes) in our study remains enigmatic. SIFa_R2 in endomembranes may utilize GPCR endosomal signaling (Liccardo et al., 2022) or simply be undergoing cellular trafficking to or from the cell membrane. In addition, we speculate that the lack of SIFa_R2 immunoreactivity in type II acini in partially-fed females may correspond to a stage-specific feature during the feeding period. Nevertheless, it is important to highlight that in the current study we use an anti-peptide SIFa_R2 antibody targeting the intracellular C-terminal of the protein. This approach resulted in strong but slightly unexpected immunostaining of cell organelle endomembranes in both salivary glands from partially-fed females as well as CHO cells expressing the receptor. Here, a western blot for the membrane protein will be required for further confirmation of antibody specificity, although our preliminary trial of this technique was inconclusive. Therefore, future experimental work to confirm and clarify the immunolabeling results obtained in current study would be beneficial.

Saliva secretory activity of type II and III acini ensures the tick's biological success during both off- and on-host stages (Kim et al., 2014, 2016; Mateos-Hernandéz et al., 2020a; Šimo et al., 2017) thus the presence of SIFamide in axon terminals (Šimo et al., 2013) along with the SIFa_R2 protein (this study) in unfed as well as partially-fed *I. ricinus* females suggest the importance of SIFamide control of GCs during both these periods. At this time, there is little understanding about how particular acini types functionally contribute to saliva content via their secretory cells, as the tick research community currently restricts their analysis to the complex saliva cocktail (Aounallah et al., 2020; Šimo et al., 2017). Although it is generally believed that granular type II and III acini possess similar morphological features, apparent differences in number as well as types of GCs have been demonstrated (Binnington, 1978; Fawcett et al., 1981; Vancová et al., 2019). Therefore, we speculate that SIFamide signaling may control basal GCs in either type II or III acini for the secretion of different substances with distinct biological functions, although this assumption requires additional experimental confirmation.

Based on current results and our previous reports (Vancová et al., 2019) we suggest that in *I. ricinus* type II and III salivary gland acini, SIFamide released from the axon terminals acts via the two surface receptor types to regulate different basally located cells: i) both SIFa_R1 and SIFa_R2 control the acinar valve via ECs and MC activity, ii) SIFa_R1 may be implicated in the neuromodulation of axonal projections adjoining SIFamide axons, iii) SIFa_R2 may act as an autoreceptor in SIFamide-axon terminals, and iv) SIFa_R2 may regulate the activity of basal GCs.

The basal parts of type II and III acini are composed of various convoluted cells surrounding the chitinous acinar duct and valve, as well as intertwingled neuropeptidergic axons forming synaptic connections with specific cell types (Vancová et al., 2019). The single PcSG cell origin of neuropeptide signaling in type II and III acini (Šimo et al., 2009b) has led to the hypothesis that this region is under synchronized peptidergic control in several hundred types of granular acini. The acinar basal region has considerable structural complexity as it is targeted by at least three classes of neuropeptides (Kim et al., 2018; Šimo et al., 2009b). The intricacy of this apparatus, in tandem with axon terminal activity and strict regulation of cell-surface protein expression in postsynaptic cells, suggest that these systems are the crucial regulatory mechanisms for synchronized or selective control of saliva-producing acini in hard tick salivary glands.

Formatting of funding sources

This study was supported by the French National Research Agency (ANR) [grant number: ANR-21-CE14-0012], project AxoTick. UMR BIPAR is supported by the French Government's *Investissement d'Avenir* program, *Laboratoire d'Excellence* "Integrative Biology of Emerging Infectious Diseases" [grant number: ANR-10-LABX-62-IBEID]. Ondrej Hajdusek and Jan Perner were supported by the "Centre for research of pathogenicity and virulence of parasites" [grant number: CZ.02.1.01/0.0/0.0/16_019/0000759] funded by the European Regional Development Fund (ERDF) and Ministry of Education, Youth, and Sport (MEYS) and additionally J.P. by the Czech Science Foundation grant [grant number: Nos. 22–18424M]. Laboratory of electron microscopy (Biology Centre) was supported by MEYS CR Czech BioImaging grant [grant number: LM2018129].

CRediT author statement

Ladislav Šimo: Conceptualization, methodology, validation, formal analysis, investigation, writing - original draft preparation, visualization, funding acquisition. **Fetta Guerrib**, **Caina Ning**, **Lourdes Mateos-Hernandéz**, **Sabine Rakotobe**, **Ondrej Hajdusek**, **Jan Perner, Marie Vancová, James J. Valdés:** Investigation, formal analysis, **Yoonseong Park:** Resources.

Acknowledgements

We are grateful to Jan Veenstra from the University of Bordeaux, France, for providing the anti-SIFamide antibody and for critical review of earlier manuscript versions. We thank Martina Tesařová from the Biology Centre, Czech Academy of Sciences, Czech Republic for technical assistance with immunogold labeling.

Appendix A. Supplementary data

Supplementary data to this article can be found online at https://doi.org/10.1016/j.ibmb.2023.103963.

References

Almazán, C., Bonnet, S., Cote, M., Slovák, M., Park, Y., Šimo, L., 2018. A versatile model of hard tick infestation on laboratory rabbits. JoVE, e57994. https://doi.org/10.3791/57994.

Aounallah, H., Bensaoud, C., M'ghirbi, Y., Faria, F., Chmelař, J., Kotsyfakis, M., 2020. Tick salivary compounds for targeted immunomodulatory therapy. Front. Immunol. 11.

Berman, H.M., Westbrook, J., Feng, Z., Gilliland, G., Bhat, T.N., Weissig, H., Shindyalov, I.N., Bourne, P.E., 2000. The protein data bank. Nucleic Acids Res. 28, 235–242. https://doi.org/10.1093/nar/28.1.235.

Binnington, K.C., 1978. Sequential changes in salivary gland structure during attachment and feeding of the cattle tick, Boophilus microplus. Int. J. Parasitol. 8, 97–115.

Bowers, K.J., Chow, D.E., Xu, H., Dror, R.O., Eastwood, M.P., Gregersen, B.A., Klepeis, J. L., Kolossvary, I., Moraes, M.A., Sacerdoti, F.D., Salmon, J.K., Shan, Y., Shaw, D.E., 2006. Scalable algorithms for molecular dynamics simulations on commodity clusters. In: SC '06: Proceedings of the 2006 ACM/IEEE Conference on Supercomputing. Presented at the SC '06: Proceedings of the 2006 ACM/IEEE Conference on Supercomputing. https://doi.org/10.1109/SC.2006.54, 43–43.

Caers, J., Verlinden, H., Zels, S., Vandersmissen, H.P., Vuerinckx, K., Schoofs, L., 2012. More than two decades of research on insect neuropeptide GPCRs: an overview. Front. Endocrinol. 3.

Calkins, T.L., Tamborindeguy, C., Pietrantonio, P.V., 2019. GPCR annotation, G proteins, and transcriptomics of fire ant (Solenopsis invicta) queen and worker brain: an improved view of signaling in an invasive superorganism. General and Comparative Endocrinology, Insect Comparative Endocrinology and Neurobiology 278, 89–103. https://doi.org/10.1016/j.ygcen.2018.12.008.

Choi, C., Cao, G., Tanenhaus, A., McCarthy, E., Jung, M., Schleyer, W., Shang, Y., Rosbash, M., Yin, J., Nitabach, M., 2012. Autoreceptor control of peptide/neurotransmitter corelease from PDF neurons determines allocation of circadian activity in Drosophila. Cell Rep. 2, 332–344. https://doi.org/10.1016/j.celrep.2012.06.021.

Dreyer, A.P., Martin, M.M., Fulgham, C.V., Jabr, D.A., Bai, L., Beshel, J., Cavanaugh, D. J., 2019. A circadian output center controlling feeding:fasting rhythms in Drosophila. PLoS Genet. 15, e1008478 https://doi.org/10.1371/journal.pgen.1008478.

Egekwu, N., Sonenshine, D.E., Garman, H., Barshis, D.J., Cox, N., Bissinger, B.W., Zhu, J., Roe, R.M., 2016. Comparison of synganglion neuropeptides, neuropeptide receptors and neurotransmitter receptors and their gene expression in response to feeding in Ixodes scapularis (Ixodidae) vs. Ornithodoros turicata (Argasidae). Insect Mol. Biol. 25, 72–92. https://doi.org/10.1111/imb.12202.

Evans, D.J., Holian, B.L., 1985. The nose–hoover thermostat. J. Chem. Phys. 83, 4069–4074. https://doi.org/10.1063/1.449071.

Fawcett, D.W., Doxsey, S.J., Buscher, G., 1981. Salivary gland of the tick vector (R. appediculatus) of East Coast Fever. II. Cellular basis for fluid secretion in the type III acinus. Tissue Cell 13, 231–253.

Gulia-Nuss, M., Nuss, A.B., Meyer, J.M., Sonenshine, D.E., Roe, R.M., Waterhouse, R.M., Sattelle, D.B., de la Fuente, J., Ribeiro, J.M., Megy, K., Thimmapuram, J., Miller, J. R., Walenz, B.P., Koren, S., Hostetler, J.B., Thiagarajan, M., Joardar, V.S., Hannick, L.I., Bidwell, S., Hammond, M.P., Young, S., Zeng, Q., Abrudan, J.L., Almeida, F.C., Ayllón, N., Bhide, K., Bissinger, B.W., Bonzon-Kulichenko, E., Buckingham, S.D., Caffrey, D.R., Caimano, M.J., Croset, V., Driscoll, T., Gilbert, D., Gillespie, J.J., Giraldo-Calderón, G.I., Grabowski, J.M., Jiang, D., Khalil, S.M.S., Kim, D., Kocan, K.M., Koči, J., Kuhn, R.J., Kurtti, T.J., Lees, K., Lang, E.G., Kennedy, R.C., Kwon, H., Perera, R., Qi, Y., Radolf, J.D., Sakamoto, J.M., Sánchez-Gracia, A., Severo, M.S., Silverman, N., Šimo, L., Tojo, M., Tornador, C., Van Zee, J. P., Vázquez, J., Vieira, F.G., Villar, M., Wespiser, A.R., Yang, Y., Zhu, J., Arensburger, P., Pietrantonio, P.V., Barker, S.C., Shao, R., Zdobnov, E.M., Hauser, F., Grimmelikhuijzen, C.J.P., Park, Y., Rozas, J., Benton, R., Pedra, J.H.F., Nelson, D.R., Unger, M.F., Tubio, J.M.C., Tu, Z., Robertson, H.M., Shumway, M., Sutton, G., Wortman, J.R., Lawson, D., Wikel, S.K., Nene, V.M., Fraser, C.M., Collins, F.H., Birren, B., Nelson, K.E., Caler, E., Hill, C.A., 2016. Genomic insights into the Ixodes scapularis tick vector of Lyme disease. Nat. Commun. 7, 10507 https://doi.org/10.1038/ncomms10507.

Holmes, S.P., Barhoumi, R., Nachman, R.J., Pietrantonio, P.V., 2003. Functional analysis of a G protein-coupled receptor from the southern cattle tick Boophilus microplus (Acari: ixodidae) identifies it as the first arthropod myokinin receptor. Insect Mol. Biol. 12, 27–38. https://doi.org/10.1046/j.1365-2583.2003.00384.x.

Holmes, S.P., He, H., Chen, A.C., lvie, G.W., Pietrantonio, P.V., 2000. Cloning and transcriptional expression of a leucokinin-like peptide receptor from the southern cattle tick, Boophilus microplus (Acari: ixodidae). Insect Mol. Biol. 9, 457–465. https://doi.org/10.1046/j.1365-2583.2000.00208.x.

Hong, C., Byrne, N.J., Zamlynny, B., Tummala, S., Xiao, L., Shipman, J.M., Partridge, A. T., Minnick, C., Breslin, M.J., Rudd, M.T., Stachel, S.J., Rada, V.L., Kern, J.C., Armacost, K.A., Hollingsworth, S.A., O'Brien, J.A., Hall, D.L., McDonald, T.P., Strickland, C., Brooun, A., Soisson, S.M., Hollenstein, K., 2021. Structures of active-state orexin receptor 2 rationalize peptide and small-molecule agonist recognition and receptor activation. Nat. Commun. 12, 815. https://doi.org/10.1038/s41467-021-21087-6.

Huang, J., MacKerell Jr., A.D., 2013. CHARMM36 all-atom additive protein force field: validation based on comparison to NMR data. J. Comput. Chem. 34, 2135–2145. https://doi.org/10.1002/jcc.23354.

Humphrey, W., Dalke, A., Schulten, K., 1996. VMD: Visual molecular dynamics. J. Mol. Graph. 14, 33–38. https://doi.org/10.1016/0263-7855(96)00018-5.

Jørgensen, L.M., Hauser, F., Cazzamali, G., Williamson, M., Grimmelikhuijzen, C.J.P., 2006. Molecular identification of the first SIFamide receptor. Biochem. Biophys. Res. Commun. 340, 696–701. https://doi.org/10.1016/j.bbrc.2005.12.062.

Jorgensen, W.L., Chandrasekhar, J., Madura, J.D., Impey, R.W., Klein, M.L., 1983. Comparison of simple potential functions for simulating liquid water. J. Chem. Phys. 79, 926–935. https://doi.org/10.1063/1.445869.

Kaufman, W.R., Phillips, J.E., 1973. Ion and water balance in the ixodid tick Dermacentor andersoni. I. Routes of ion and water excretion. J. Exp. Biol. 58, 523–536.

Kelley, L.A., Mezulis, S., Yates, C.M., Wass, M.N., Sternberg, M.J.E., 2015. The Phyre2 web portal for protein modeling, prediction and analysis. Nat. Protoc. 10, 845–858. https://doi.org/10.1038/nprot.2015.053.

Kim, D., Šimo, L., Park, Y., 2018. Molecular characterization of neuropeptide elevenin and two elevenin receptors, IsElevR1 and IsElevR2, from the blacklegged tick, Ixodes scapularis. Insect Biochem. Mol. Biol. 101, 66–75. https://doi.org/10.1016/j.ibmb.2018.07.005.

Kim, D., Šimo, L., Park, Y., 2014. Orchestration of salivary secretion mediated by two different dopamine receptors in the blacklegged tick Ixodes scapularis. J. Exp. Biol. 217, 3656–3663. https://doi.org/10.1242/jeb.109462.

Kim, D., Šimo, L., Vancová, M., Urban, J., Park, Y., 2019. Neural and endocrine regulation of osmoregulatory organs in tick: recent discoveries and implications. Gen. Comp. Endocrinol. 278, 42–49. https://doi.org/10.1016/j.ygcen.2018.08.004.

Kim, D., Urban, J., Boyle, D.L., Park, Y., 2016. Multiple functions of Na/K-ATPase in dopamine-induced salivation of the Blacklegged tick, Ixodes scapularis. Sci. Rep. 6, 21047 https://doi.org/10.1038/srep21047.

Koči, J., Šimo, L., Park, Y., 2013. Validation of internal reference genes for real-time quantitative polymerase chain reaction studies in the tick, Ixodes scapularis (Acari: ixodidae). J. Med. Entomol. 50, 79–84. https://doi.org/10.1603/me12034.

Krissinel, E., Henrick, K., 2007. Inference of macromolecular assemblies from crystalline state. J. Mol. Biol. 372, 774–797. https://doi.org/10.1016/j.jmb.2007.05.022.

Liccardo, F., Luini, A., Di Martino, R., 2022. Endomembrane-based signaling by GPCRs and G-proteins. Cells 11, 528. https://doi.org/10.3390/cells11030528.

Livak, K.J., Schmittgen, T.D., 2001. Analysis of relative gene expression data using real-time quantitative PCR and the 2(-Delta Delta C(T)) Method. Methods 25, 402–408. https://doi.org/10.1006/meth.2001.1262.

Mahoney, M.W., Jorgensen, W.L., 2000. A five-site model for liquid water and the reproduction of the density anomaly by rigid, nonpolarizable potential functions. J. Chem. Phys. 112, 8910–8922. https://doi.org/10.1063/1.481505.

Mans, B.J., 2019. Chemical equilibrium at the tick–host feeding interface:A critical examination of biological relevance in hematophagous behavior. Front. Physiol. 10.

Martelli, C., Pech, U., Kobbenbring, S., Pauls, D., Bahl, B., Sommer, M.V., Pooryasin, A., Barth, J., Arias, C.W.P., Vassiliou, C., Luna, A.J.F., Poppinga, H., Richter, F.G., Wegener, C., Fiala, A., Riemensperger, T., 2017. SIFamide translates hunger signals into appetitive and feeding behavior in Drosophila. Cell Rep. 20, 464–478. https://doi.org/10.1016/j.celrep.2017.06.043.

Martyna, G.J., Tobias, D.J., Klein, M.L., 1994. Constant pressure molecular dynamics algorithms. J. Chem. Phys. 101, 4177–4189. https://doi.org/10.1063/1.467468.

Mateos-Hernandéz, L., Defaye, B., Vancová, M., Hajdusek, O., Sima, R., Park, Y., Attoui, H., Šimo, L., 2020a. Cholinergic axons regulate type I acini in salivary glands of Ixodes ricinus and Ixodes scapularis ticks. Sci. Rep. 10, 16054 https://doi.org/10.1038/s41598-020-73077-1.

Mateos-Hernández, L., Pipová, N., Allain, E., Henry, C., Rouxel, C., Lagrée, A.-C., Haddad, N., Boulouis, H.-J., Valdés, J.J., Alberdi, P., de la Fuente, J., Cabezas-Cruz, A., Šimo, L., 2021. Enlisting the Ixodes scapularis embryonic ISE6 cell line to investigate the neuronal basis of tick-pathogen interactions. Pathogens 10, 70. https://doi.org/10.3390/pathogens10010070.

Mateos-Hernández, L., Rakotobe, S., Defaye, B., Cabezas-Cruz, A., Šimo, L., 2020b. A capsule-based model for immature hard tick stages infestation on laboratory mice. J. Vis. Exp. https://doi.org/10.3791/61430.

Perner, J., Helm, D., Haberkant, P., Hatalova, T., Kropackova, S., Ribeiro, J.M., Kopacek, P., 2020. The central role of salivary metalloproteases in host acquired resistance to tick feeding. Front. Cell. Infect. Microbiol. 10.

Pierce, K.L., Premont, R.T., Lefkowitz, R.J., 2002. Seven-transmembrane receptors. Nat. Rev. Mol. Cell Biol. 3, 639–650. https://doi.org/10.1038/nrm908.

Pietrantonio, P.V., Xiong, C., Nachman, R.J., Shen, Y., 2018. G protein-coupled receptors in arthropod vectors: omics and pharmacological approaches to elucidate ligand-receptor interactions and novel organismal functions. Current Opinion in Insect Science, Global change biology * Molecular physiology 29, 12–20. https://doi.org/10.1016/j.cois.2018.05.016.

Roller, L., Yamanaka, N., Watanabe, K., Daubnerová, I., Žitňan, D., Kataoka, H., Tanaka, Y., 2008. The unique evolution of neuropeptide genes in the silkworm Bombyx mori. Insect Biochem. Mol. Biol. 38, 1147–1157. https://doi.org/10.1016/j.ibmb.2008.04.009.

Sastry, G.M., Adzhigirey, M., Day, T., Annabhimoju, R., Sherman, W., 2013. Protein and ligand preparation: parameters, protocols, and influence on virtual screening enrichments. J. Comput. Aided Mol. Des. 27, 221–234. https://doi.org/10.1007/s10822-013-9644-8.

Schrödinger Release 2022-1, 2021. Maestro, Schrödinger, LLC, New York, NY.

Schwyzer, R., 1977. Acth: a short introductory review. Ann. N. Y. Acad. Sci. 297, 3–26. https://doi.org/10.1111/j.1749-6632.1977.tb41843.x.

Sellami, A., Veenstra, J.A., 2015. SIFamide acts on fruitless neurons to modulate sexual behavior in Drosophila melanogaster. Peptides 74, 50–56. https://doi.org/10.1016/j.peptides.2015.10.003.

Šimo, L., Sonenshine, D.E., Park, Y., Žitňan, D., 2014a. The nervous and sensory systems: structure, function, proteomics and genomics. In: Sonenshine, D.E., Roe, R.M. (Eds.), Biology of Ticks. Oxford University Press, New York, pp. 309–367.

Šimo, L., Kazimirova, M., Richardson, J., Bonnet, S.I., 2017. The essential role of tick salivary glands and saliva in tick feeding and pathogen transmission. Front. Cell. Infect. Microbiol. 7.

Šimo, L., Koči, J., Kim, D., Park, Y., 2014b. Invertebrate specific D1-like dopamine receptor in control of salivary glands in the black-legged tick Ixodes scapularis. J. Comp. Neurol. 522, 2038–2052. https://doi.org/10.1002/cne.23515.

Šimo, L., Koči, J., Park, Y., 2013. Receptors for the neuropeptides, myoinhibitory peptide and SIFamide, in control of the salivary glands of the blacklegged tick Ixodes

scapularis. Insect Biochem. Mol. Biol. 43, 376–387. https://doi.org/10.1016/j.ibmb.2013.01.002.

Šimo, L., Koči, J., Žitňan, D., Park, Y., 2011. Evidence for D1 dopamine receptor activation by a paracrine signal of dopamine in tick salivary glands. PLoS One 6, e16158. https://doi.org/10.1371/journal.pone.0016158.

Šimo, L., Park, Y., 2014. Neuropeptidergic control of the hindgut in the black-legged tick Ixodes scapularis. Int. J. Parasitol. 44, 819–826. https://doi.org/10.1016/j.ijpara.2014.06.007.

Šimo, L., Slovák, M., Park, Y., Žitňan, D., 2009a. Identification of a complex peptidergic neuroendocrine network in the hard tick, Rhipicephalus appendiculatus. Cell Tissue Res. 335, 639–655. https://doi.org/10.1007/s00441-008-0731-4.

Šimo, L., Žitňan, D., Park, Y., 2009b. Two novel neuropeptides in innervation of the salivary glands of the black-legged tick, Ixodes scapularis: myoinhibitory peptide and SIFamide. J. Comp. Neurol. 517, 551–563. https://doi.org/10.1002/cne.22182.

Tamura, K., Stecher, G., Kumar, S., 2021. MEGA11: molecular evolutionary genetics analysis version 11. Mol. Biol. Evol. 38, 3022–3027. https://doi.org/10.1093/molbev/msab120.

Terhzaz, S., Rosay, P., Goodwin, S.F., Veenstra, J.A., 2007. The neuropeptide SIFamide modulates sexual behavior in Drosophila. Biochem. Biophys. Res. Commun. 352, 305–310. https://doi.org/10.1016/j.bbrc.2006.11.030.

Tikhonova, I.G., Gigoux, V., Fourmy, D., 2019. Understanding peptide binding in class A G protein-coupled receptors. Mol. Pharmacol. 96, 550–561. https://doi.org/10.1124/mol.119.115915.

Tuckerman, M., Berne, B.J., Martyna, G.J., 1992. Reversible multiple time scale molecular dynamics. J. Chem. Phys. 97, 1990–2001. https://doi.org/10.1063/1.463137.

Vancová, M., Bílý, T., Nebesářová, J., Grubhoffer, L., Bonnet, S., Park, Y., Šimo, L., 2019. Ultrastructural mapping of salivary gland innervation in the tick Ixodes ricinus. Sci. Rep. 9, 6860. https://doi.org/10.1038/s41598-019-43284-6.

Veenstra, J.A., 2021. The neuropeptide SMYamide, a SIFamide paralog, is expressed by salivary gland innervating neurons in the American cockroach and likely functions as a hormone. Peptides 136, 170466. https://doi.org/10.1016/j.peptides.2020.170466.

Verleyen, P., Huybrechts, J., Baggerman, G., Van Lommel, A., De Loof, A., Schoofs, L., 2004. SIFamide is a highly conserved neuropeptide: a comparative study in different insect species. Biochem. Biophys. Res. Commun. 320, 334–341. https://doi.org/10.1016/j.bbrc.2004.05.173.

Verlinden, H., Gijbels, M., Lismont, E., Lenaerts, C., Vanden Broeck, J., Marchal, E., 2015. The pleiotropic allatoregulatory neuropeptides and their receptors: a mini-review. J. Insect Physiol. 80, 2–14. https://doi.org/10.1016/j.jinsphys.2015.04.004.

Vernon, W.I., Printen, J.A., 2002. Assay for intracellular calcium using a codon-optimized aequorin. Biotechniques 33, 730. https://doi.org/10.2144/02334bm02, 732, 734.

Yang, J., Zhang, Y., 2015. I-TASSER server: new development for protein structure and function predictions. Nucleic Acids Res. 43, W174–W181. https://doi.org/10.1093/nar/gkv342.

Yang, Y., Bajracharya, P., Castillo, P., Nachman, R.J., Pietrantonio, P.V., 2013. Molecular and functional characterization of the first tick CAP2b (periviscerokinin) receptor from Rhipicephalus (Boophilus) microplus (Acari: ixodidae). Gen. Comp. Endocrinol. 194, 142–151. https://doi.org/10.1016/j.ygcen.2013.09.001.

Zhou, P., Jin, B., Li, H., Huang, S.-Y., 2018. HPEPDOCK: a web server for blind peptide-protein docking based on a hierarchical algorithm. Nucleic Acids Res. 46, W443–W450. https://doi.org/10.1093/nar/gky357.

Zhu, J., Fan, H., Periole, X., Honig, B., Mark, A.E., 2008. Refining homology models by combining replica-exchange molecular dynamics and statistical potentials. Proteins: Struct., Funct., Bioinf. 72, 1171–1188. https://doi.org/10.1002/prot.22005.